ROM SAF Report 22
Ref: SAF/ROM/METO/REP/RSR/022
Web: www.romsaf.org
Date: 27 August 2015

The EUMETSAT Network of Satellite Application Facilities

ROM SAF
Radio Occultation Meteorology

ROM SAF Report 22

The use of the GPS radio occultation reflection flag for NWP applications

Sean Healy

ECMWF

Document Author Table

	Name	Function	Date	Comments
Prepared by:	S. Healy	ROM SAF Project Team	27 August 2015	
Reviewed by:	C. Burrows	ROM SAF Project Team	4 September 2015	
Reviewed by:	-	-	-	
Approved by:	K. B. Lauritsen	ROM SAF Project Manager	20 October 2015	

Document Change Record

Issue/Revision	Date	By	Description
1.0	7 September, 2015	S. Healy	Minor changes following first review
1.1	21 October, 2015	S. Healy	Minor changes required for release

ROM SAF

The Radio Occultation Meteorology Satellite Application Facility (ROM SAF) is a decentralised processing centre under EUMETSAT which is responsible for operational processing of GRAS radio occultation data from the Metop satellites and RO data from other missions. The ROM SAF delivers bending angle, refractivity, temperature, pressure, and humidity profiles in near-real time and offline for NWP and climate users. The offline profiles are further processed into climate products consisting of gridded monthly zonal means of bending angle, refractivity, temperature, humidity, and geopotential heights together with error descriptions.

The ROM SAF also maintains the Radio Occultation Processing Package (ROPP) which contains software modules that will aid users wishing to process, quality-control and assimilate radio occultation data from any radio occultation mission into NWP and other models.

The ROM SAF Leading Entity is the Danish Meteorological Institute (DMI), with Cooperating Entities: i) European Centre for Medium-Range Weather Forecasts (ECMWF) in Reading, United Kingdom, ii) Institut D'Estudis Espacials de Catalunya (IEEC) in Barcelona, Spain, and iii) Met Office in Exeter, United Kingdom. To get access to our products or to read more about the project please go to: http://www.romsaf.org

Intellectual Property Rights

All intellectual property rights of the ROM SAF products belong to EUMETSAT. The use of these products is granted to every interested user, free of charge. If you wish to use these products, EUMETSAT's copyright credit must be shown by displaying the words "copyright (year) EUMETSAT" on each of the products used.

Abstract

A COSMIC dataset has been modified by IEEC and the Met Office to include a reflection flag. The flagged measurements are composed of a direct and reflected signal. They have been detected automatically using a technique developed by IEEC. The error statistics of the COSMIC data subsets with and without the flag activated have been computed in data assimilation experiments. It has been confirmed that the bending angle departure statistics of measurements in the troposphere with the flag activated tend to fit ECMWF forecasts more closely. However, the variability of the observations in the flagged subset is much lower, and the flag is more probable for colder, drier tropospheres. The improvement in the departure statistics varies spatially, indicating that a simple scaling of the bending error statistics used to assimilate the data when the flag is activated, is probably not appropriate. This will complicate any use of a single on/off flag in NWP applications.

Contents

1 Chapter

1.1 Introduction

The ability to identify GPS radio occultation (GPS-RO) observations with smaller errors is of potential interest to NWP users, because these observations could be given greater weight in the data assimilation process. Research performed at IEEC (Cardellach *et al.*, 2008; Cardellach and Oliveras, 2015), automatically identifying occultations which contain both a direct and reflected signal (E.g., see Beyerle and Hocke, 2001), has indicated that refractivity profiles derived from these observations agree more closely with ECMWF short-range forecasts than the refractivity profiles derived from observations that contain only one direct signal. This is a potentially interesting result, indicating that the GPS-RO errors are smaller in the reflection cases, but it is counter-intuitive. One may naively *assume* that cases where reflections were present would have larger observation errors because the reflected signals would complicate the measurement of the direct signal.

Although it is unclear physically why the flagged measurements, containing both a direct and reflected signal, have better error characteristics, IEEC have noted the following in relation to the probability of occurrence of the flag:

- Around $\sim 36\%$ of all observations are flagged as containing both a direct and reflected signal. The percentage over oceans increases to $\sim 45\%$.
- The flagged measurements mainly occur over ocean or ice surfaces. The percentage over ocean varies with latitude, with a higher percentage of flagged events at higher latitudes.
- An occultation must reach the lowest levels of the atmosphere to be flagged, but this alone does not guarantee a reflection event.
- There is a seasonal signal in the percentage of flagged events. The percentage of flagged measurements is smaller in summer than in winter.
- There is a weak negative correlation between obtaining a reflection flag and increasing temperature in the lower troposphere.
- There is a weak negative correlation between obtaining a reflection flag and increasing humidity in the lower troposphere.
- There is a weak negative correlation between obtaining a reflection flag and increasing sea surface temperature.

- Ocean surface winds or roughness are not correlated with the occurrence of a flagged measurement.

This report summarizes results from a ROM SAF CDOP-2 workpackage, which aims to investigate the potential utility of an on/off reflection "flag" for NWP applications. We are interested if the reflection flag provides useful, additional information that could be used during the data assimilation process. This would justify introducing the detection of reflections in the operational GPS-RO processing, and including the flag in the operational BUFR files. More specifically, the aim has been to investigate whether the on/off reflection flag can be used to adjust the *assumed* observation covariance matrix, $\mathbf{R_a}$.

In this study, we essentially reproduce the main IEEC results showing that reflected measurements fit ECMWF short-range forecasts more closely. However, we find that this improvement in the departure statistics is not spatially uniform, indicating that simple scaling of the of the assumed error covariance matrix when a reflection is detected is probably not appropriate. Furthermore, it is shown that the observation variablity is significantly lower in the flagged dataset, and the mean tropospheric bending angles are smaller when the reflections occur.

The main results are presented in section 1.2, and the discussion and conclusions are given in section 1.3.

1.2 Method and Main Results

This study is based on a COSMIC dataset modified by IEEC and the Met Office. The dataset covers the period November 1 to December 31, 2008. The measurements with a reflection were identified at IEEC using a Support Vector Machine (SVM) supervised learning approach, as outlined in Cardellach *et al.* (2008) and Cardellach and Oliveras (2015). It produces a scalar for each occultation, which is related to the probability of receiving both a direct and reflected signal. In this study, a SVM scalar value > 0.25 is used to identify and flag the cases where both direct and reflected signals are measured, and these will be referred to as "Ref" or flagged cases. If the SVM flag < 0.25, the flag is not activiated because there is just a direct signal. If the flag is not activated, the GPS-RO measurement will be referred to as a "NoRef" case.

The BUFR files used in the experiment were modified by the Met Office to include the reflection flag. In total, 38542 ($\sim 35\%$) profiles are flagged (Ref), and 70550 are not flagged (NoRef).

The probability of a flagged occultation as a function of latitude for "all data", and just the subset over sea, is shown in Figure 1.1. This is consistent with previous work at IEEC (Cardellach and Oliveras, 2015), where it is noted that the Ref measurements occur mainly over sea or ice, and the NoRef data is more evenly distributed spatially.

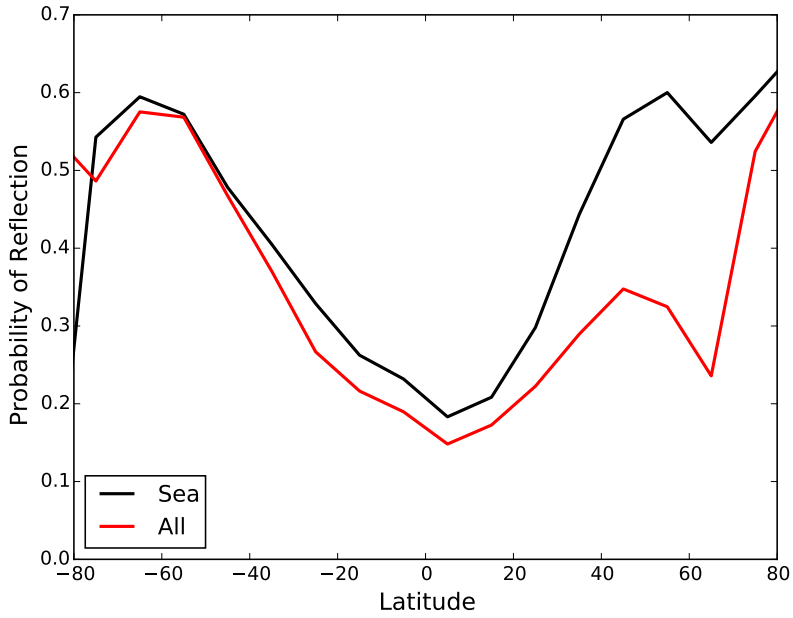

Figure 1.1: The probability of a reflected event as a function of latitude for all data and only measurements over sea. The period is November 1 to December 31, 2008.

Estimating the observation error statistics

The estimate of the observation uncertainty is based on standard data assimilation diagnostics. It can be shown (Desroziers *et al.*, 2005) that departure statistics from assimilation experiments provide an *estimate* of the observation error covariance matrix, $\mathbf{R_D}$. More specifically, we compute

$$\mathbf{R_D} \simeq \overline{(\mathbf{y} - H(\mathbf{x_b}))(\mathbf{y} - H(\mathbf{x_a}))^T} \tag{1.1}$$

where $\mathbf{x_b}$ and $\mathbf{x_a}$ are the background forecast and analysis, respectively, H is the one dimensional bending angle forward model (Healy and Thépaut, 2006: Burrows *et al.* 2014) and $\mathbf{y}$ is the observation vector. Strictly, this expression only achieves equality if the correct covariance matrices are already known, and used to estimate the analysis, $\mathbf{x_a}$. However, the approach is useful for updating and improving the assumed observation error covariance matrix, $\mathbf{R_a}$, used to assimilate the data. In the case of GPS-RO, it provides correlation matrices that appear physically plausible given the standard GPS-RO processing steps from phase delay to bending angle.

In the experiment, we assimilate both the Ref and NoReF datasets with the same assumed error covariance matrix, $\mathbf{R_a}$. We then use Eq.1.1 to estimate the error statistics for the two data subsets. The assumed bending angle error statistics are those used operationally at ECMWF. A single covariance matrix is used globally for all GPS-RO instruments. The standard deviations of the observation errors are assumed to vary with impact height, h(=impact parameter minus radius of curvature). The percentage error is assumed to be 20% of the observed value at $h = 0$, falling linearly with h to 1% at $h = 10$ km. Above 10 km, the error is assumed to be 1% of the observed value until this reaches a lower limit of 3×10^{-6}radians. Vertical error correlations are currently ignored. Estimates of the correlations are produced

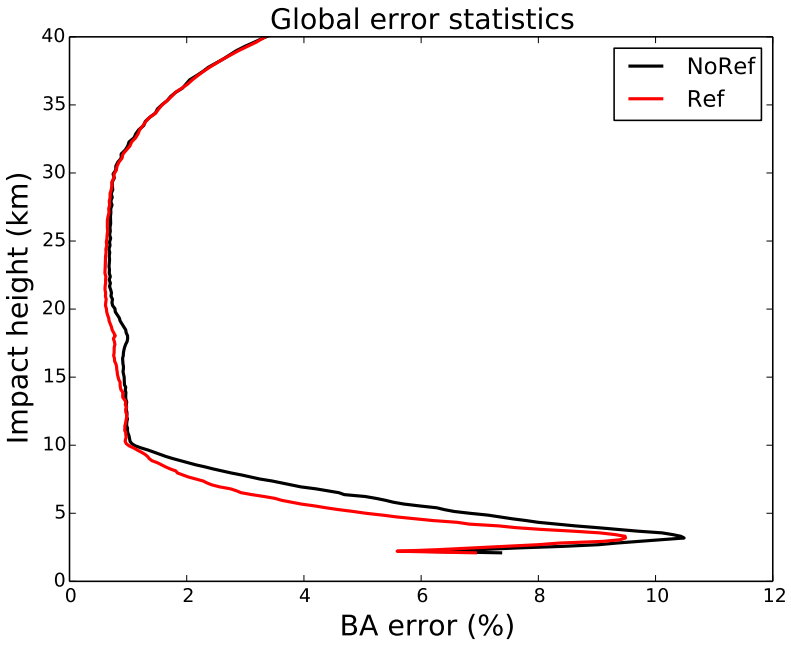

Figure 1.2: a) The globally averaged error estimates for the reflected (Ref) and non-reflected (NoRef) datasets. The period is November 1-30, 2008.

with $\mathbf{R_D}$, but they will not be discussed further here.

Figure 1.2 shows the estimated standard deviation of the globally averaged bending angle errors, produced with Eq.1.1 for the two datasets for the period November 1-30, 2008. This figure confirms the main IEEC result – but now in bending angle space – that the flagged data fit ECMWF short-range forecasts more closely, and the estimated error statistics are smaller. The improvement is most apparent below 10 km, but there is some reduction between 15 - 20 km. The reduction between 15 - 20 km is surprising, because the reflections are thought to relate to tropospheric characteristics. In fact, the uncertainty reduction in this vertical interval is a sampling issue, related to the smaller number of Ref measurements in the tropics. It is well known from monitoring at `http://www.romsaf.org/monitoring/index.php` that bending angle departure statistics tend to be larger near the tropical tropopause. There are simply more of these cases in the “NoRef” statistics, because of the distribution of observations. Figure 1.3 shows the error estimates using just departure statistics in the tropics, and the improved consistency above 10 km is clear in this case. The Ref measurement statistics are noisier because of the lower data numbers.

We have found that reflections tend to occur in cooler, drier conditions. Figure 1.4 shows the zonally averaged short-range forecasts of total column water vapour and 2 metre temperatures for the observation locations over sea for the both Ref and NoRef measurements. In general, the Ref measurements have larger total column water vapour values, except in the band between the equator and 10 degrees north. However, the data numbers are very different in this band (Figure 1.1). The NoRef minus Ref differences in the total column water are larger in the southern hemisphere than in the northern hemisphere.

An alternative way of looking at this is to plot the probability of obtaining a reflection flag, given the total column water vapour value. Figure 1.5 shows a fairly linear relationship up

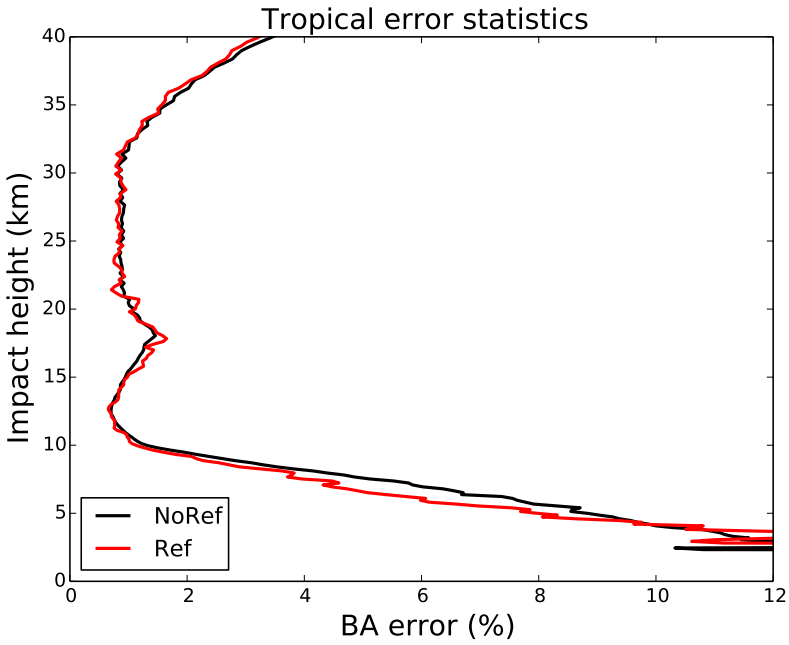

Figure 1.3: As Figure 1.2 but computing the statistics for just the tropical region.

to $\sim$ 50 kg/m^2, where the probability of a reflection falls as the total column water vapour increases. The relationship above 50 kg/m^2 is less clear, but the sample numbers are lower here and this may account for some noise. Note that less than 5 % of the sample have total column water vapour values greater than 50 kg/m^2, and this falls to less than 1 % for the number of samples that have total column water vapour values greater than 60 kg/m^2.

The improvements in the statistical error estimates are not spatially uniform across the globe. Figure 1.6 shows the difference in the error variance estimate for the northern hemisphere, tropics and southern hemisphere. A positive value indicates that the reflection measurements have a lower estimated variance. The improvement is largest in the southern hemisphere, and it is also notable that variances of the reflection data are larger in the tropics below $\sim$ 4 km. We believe that the improvements are larger in the southern hemisphere than in the northern hemisphere because of the abundance of atmospheric water vapour, related to the season. The flag has little impact on the $\mathbf{R}$ estimate in the polar regions (Figure 1.7), despite the significant numbers of reflected measurements. This demonstrates that the reflection flag alone does not guarantee smaller error estimates or improved (o-b) departures, and suggests that the abundance of tropospheric humidity is also likely to be a key factor in the improvements at the middle and lower latitudes.

It is interesting to note that the variability of the observations about the mean profile in the Ref and NoRef subsets is quite different. Figure 1.8 shows both the error estimates and variability of the observations about their respective mean profiles for the two subsets in the southern hemisphere, where the estimated error improvements are clearest (Figure 1.6). The variability of the reflected measurements is clearly much lower, and this is likely to have some impact on the estimated errors. In addition, it should be noted that the mean bending angle profiles for the two subsets is consistent with reflections occurring in drier, colder tropospheric conditions.

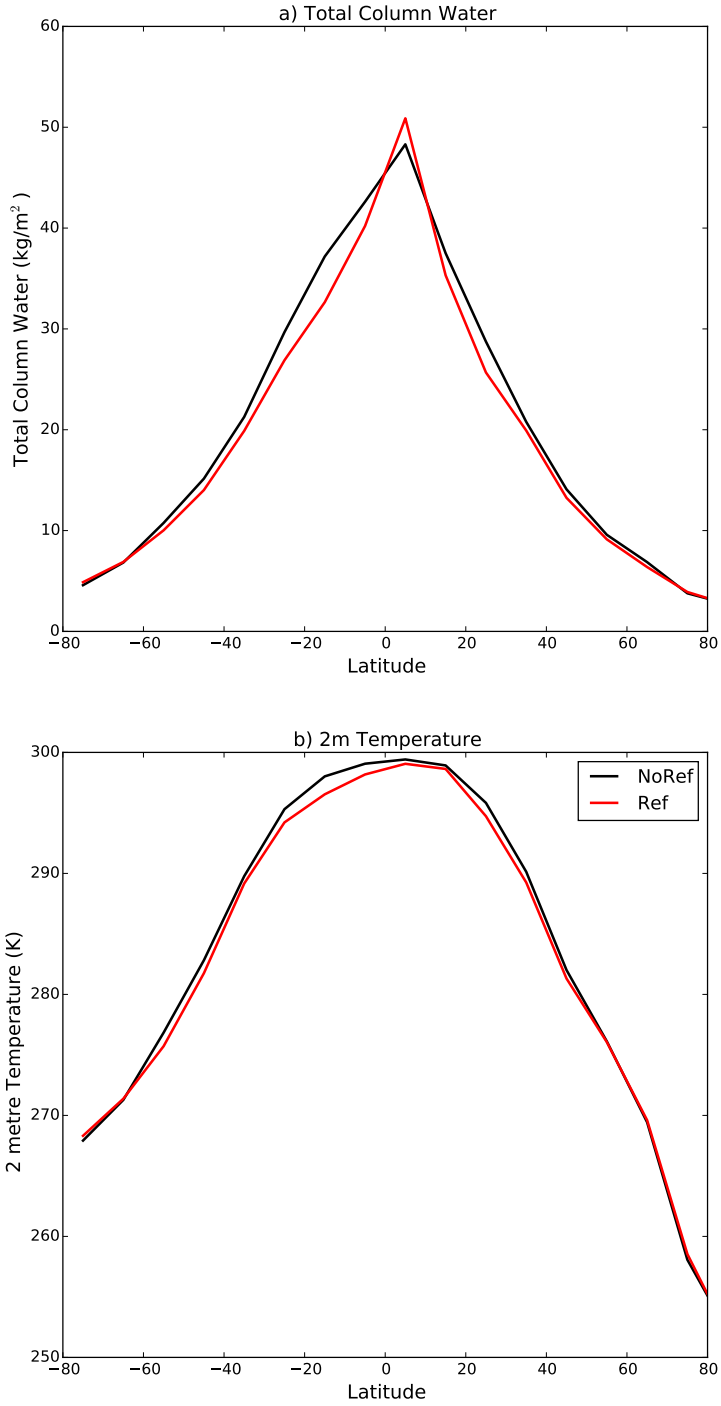

Figure 1.4: Zonally averaged a) total column water vapour and b) 2 metre temperature values at the observation locations, for measurements over the sea.

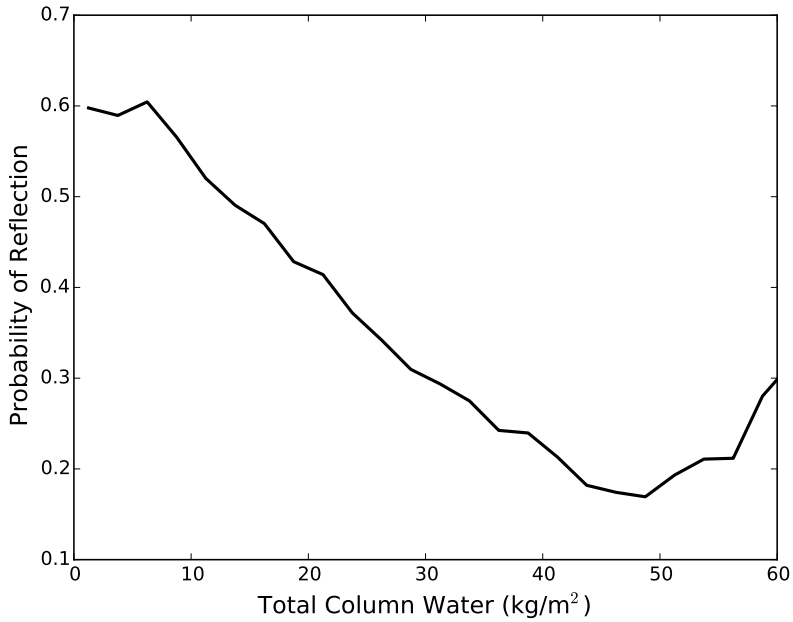

Figure 1.5: The probability of obtaining a reflection flag, for a given the total column water vapour value. The observations are over sea.

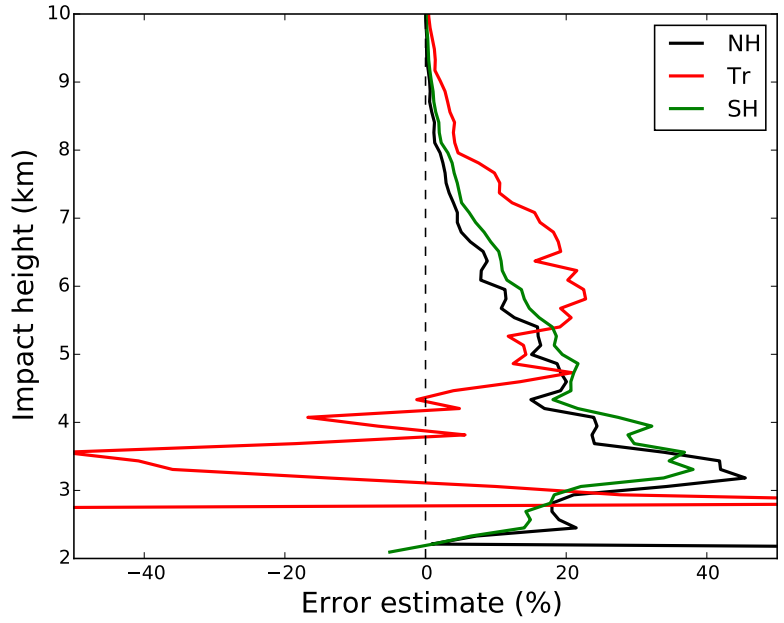

Figure 1.6: The difference in the error variance estimates (NoRef - Ref) for the northern hemisphere, tropics and southern hemisphere. A positive value indicates that the reflection data has a smaller error variance.

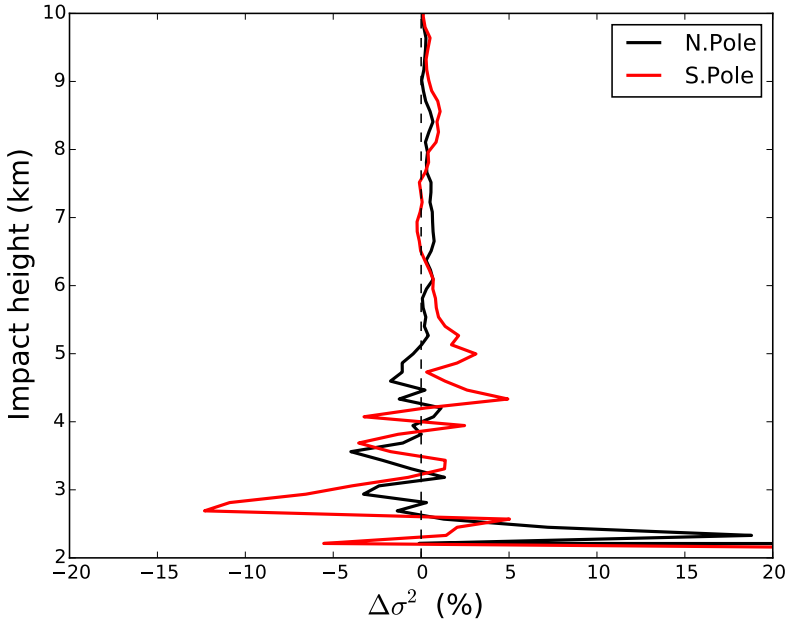

Figure 1.7: As Figure 1.6 but for the polar regions.

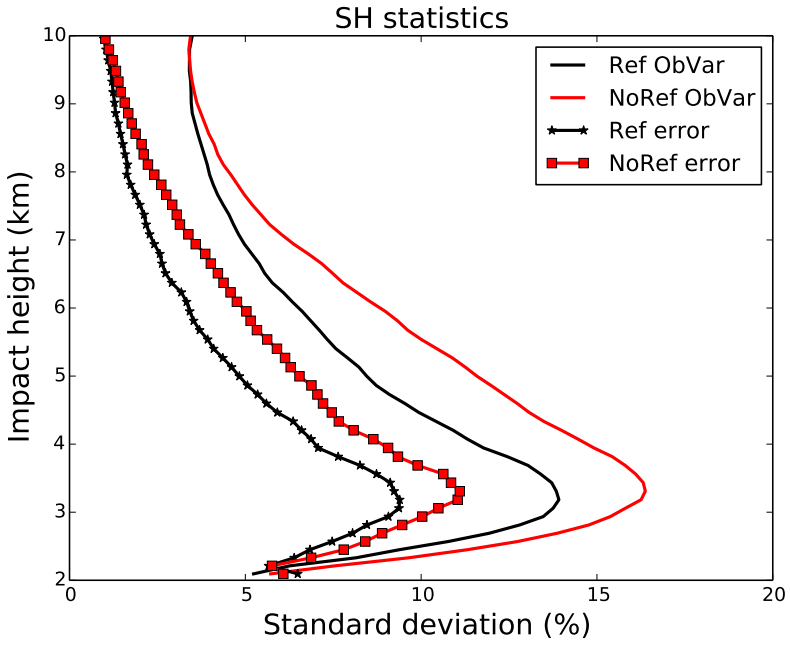

Figure 1.8: The standard deviation of the error estimates for the reflection and no reflection data and the variability of the two observation datasets about their respective mean. This is for the southern hemisphere.

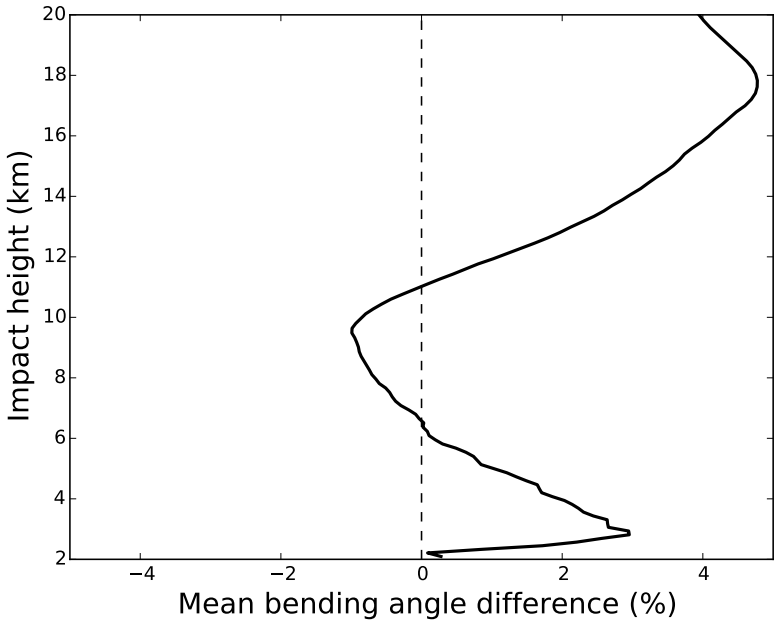

Figure 1.9: The percentage difference in the mean of the observed bending angle profiles in the southern hemisphere for the non-reflected and reflected data. The figure shows (100 $\times$ (NoRef - Ref)/NoRef).

Figure 1.9 shows the percentage difference in the mean bending angle profiles (100 $\times$ (NoRef - Ref)/NoRef) for the southern hemisphere. The difference can interpreted as follows. The NoRef cases are warmer and moister. Near the surface, the higher moisture increases the measured bending angles, whereas in the upper troposphere, the increased temperature reduces the bending angle values. In the stratosphere, the bending angles are larger because the warmer troposphere has increased the height of the fixed pressure levels through the hydrostatic integration. The difference in the mean bending angles for the northern hemisphere, tropics and southern hemisphere are shown in Figure 1.10. Note the differences in the mean profiles are smaller in the northern hemisphere than in the southern hemisphere.

The NWP forecast errors mapped to bending angle space, $\mathbf{HBH^T}$, are likely to be smaller in cold, dry conditions, but the impact of this should be removed with the use of $\mathbf{R_D}$ (Eq. 1.1). However, when the bending angles are systematically larger in the lower troposphere – as in the warmer, moister NoRef cases – the measurement signal-to-noise will be lower because of larger atmospheric defocusing. The atmospheric defocusing factor, D, is proportional to the bending angle gradient with respect to impact parameter, and it is of the form (e.g. Kursinski *et al*, 1997),

$$D \propto \frac{1}{1 - l\partial\alpha/\partial a} \tag{1.2}$$

where l is the distance from the tangent point to the receiver, and is typically $\sim$ 3000 km. Estimates of the defocusing factor could be obtained from the short-range forecast and possibly used as a predictor for the assumed error variance.

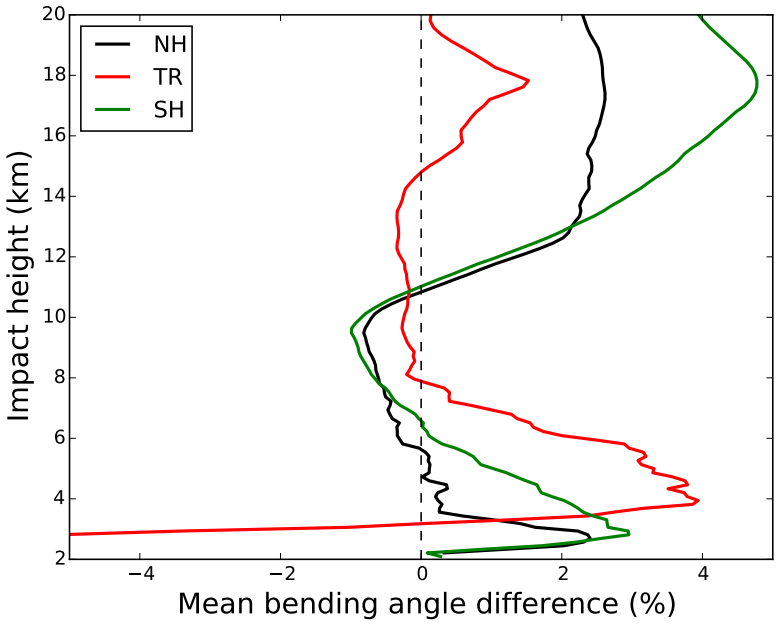

Figure 1.10: As Figure 1.9 but also showing the mean differences in the northern hemisphere (NH) and tropics (TR). The figure shows (100 $\times$ (NoRef - Ref)/NoRef).

1.3 Summary

There are three important components required to assimilate data effectively. They are:

- An accurate forward model.
- A reasonable estimate of the observation error statistics.
- A quality control system that will remove data that does not appear to be consistent with the assumed observation error statistics.

The aim of this work is to investigate whether a reflection flag can be used to improve the accuracy of the assumed error statistics used in the assimilation.

We have used the approach developed by Desrozier *et al.* (2005) to compare the bending angle error statistics of the data both with and without the reflection flag activated. It has been confirmed that data flagged as a reflection have better departure statistics in the troposphere when compared to ECMWF forecasts/analyses. The apparent improvements in the global error statistics between 15 - 20 km is simply a sampling issue.

The improvements in the departure statistics in the troposphere are not spatially uniform across the globe, and there is clearly a strong relationship with the total column water. In general, the probability of a reflection flag falls as the total column water increases (Figure 1.4). There is very little improvement in the estimated error statistics at high latitudes when the flag is on, and the improvement is larger in the southern hemisphere than in the northern hemisphere because of the season. This variation complicates the practical use of the flag in a data assimilation system. It had been hoped that the flag could be used to reduce the assumed tropospheric error statistics in a relatively simple way, perhaps by multiplying them

by a fixed scalar, but this is probably not appropriate. It is clearly questionable whether a single on/off flag can convey all the information required by an NWP user, and perhaps the scalar produced in the SVM processing might be more useful. However, this needs to be demonstrated.

Ideally, we should have a better physical understanding of why the reflected measurements produce improved departure statistics, prior to using this information in a data assimilation system. This would strengthen the case for using the flag in operational NWP. The improvement in the error estimates may the result of a number of factors which are difficult to disentangle, but the results presented here strongly suggest that the tropospheric water vapour content is a key factor. The reflected measurements tend to occur in colder and drier conditions on average, and have much lower bending angle variability than the non reflected measurements in the same area. If the error reduction is ultimately related to tropospheric humidity affecting the measurement signal to noise, then it might be possible to estimate the signal to noise and scale the assumed error statistics based on the humidity at the observation location from a short-range NWP forecast. If this can be demonstrated, the question arises:

- What is the additional information content provided by the reflection flag, relative to the information provided by a short-range NWP forecast?

This question needs to be addressed prior to any major changes in the operational GPS-RO processing and the associated BUFR template.

Acknowledgments

This work has been performed as part of ECMWF's ROM SAF CDOP-2 activities. I would like to thank Dr Estel Cardellach and Mr Dave Offiler for preparing the dataset, and Chris Burrows for reviewing the draft report.

References

Beyerle, G., and K. Hocke, 2001: Observation and simulation of direct and reflected GPS signals in radio occultation experiments. *Geophys. Res. Lett.*, **28**, 1895–1898.

Burrows, C. P., S. B. Healy, and I. D. Culverwell, 2014: Improving the bias characteristics of the ROPP refractivity and bending angle operators. *Atmos. Meas. Tech.*, **7**, 3445–3458.

Cardellach, E., and S. Oliveras, 2016: Assessment of a potential flag product. *ROM SAF Report 23*.

Cardellach, E., S. Oliveras, and A. Ruis, 2008: Applications of reflected signals found in gnss radio occultation events. *GRAS SAF Workshop on Applications of GPS radio occultation measurements*, 133–144.

Desroziers, G., L. Berre, B. Chapnik, and P. Poli, 2005: Diagnosis of observation, background and analysis-error statistics in observation space. *Q. J. R. Meteorol. Soc.*, **131**, 3385–3396.

Healy, S. B., and J.-N. Thépaut, 2006: Assimilation experiments with CHAMP GPS radio occultation measurements. *Q. J. R. Meteorol. Soc.*, **132**, 605–623.

Kursinski, E. R., G. A. Hajj, J. T. Schofield, R. P. Linfield, and K. R. Hardy, 1997: Observing earth's atmosphere with radio occultation measurements using the Global Positioning System. *J. Geophys. Res.*, **102**, 23.429–23.465.

ROM SAF (and GRAS SAF) Reports

SAF/GRAS/METO/REP/GSR/001	Mono-dimensional thinning for GPS Radio Occulation
SAF/GRAS/METO/REP/GSR/002	Geodesy calculations in ROPP
SAF/GRAS/METO/REP/GSR/003	ROPP minimiser - minROPP
SAF/GRAS/METO/REP/GSR/004	Error function calculation in ROPP
SAF/GRAS/METO/REP/GSR/005	Refractivity calculations in ROPP
SAF/GRAS/METO/REP/GSR/006	Levenberg-Marquardt minimisation in ROPP
SAF/GRAS/METO/REP/GSR/007	Abel integral calculations in ROPP
SAF/GRAS/METO/REP/GSR/008	ROPP thinner algorithm
SAF/GRAS/METO/REP/GSR/009	Refractivity coefficients used in the assimilation of GPS radio occultation measurements
SAF/GRAS/METO/REP/GSR/010	Latitudinal Binning and Area-Weighted Averaging of Irregularly Distributed Radio Occultation Data
SAF/GRAS/METO/REP/GSR/011	ROPP 1dVar validation
SAF/GRAS/METO/REP/GSR/012	Assimilation of Global Positioning System Radio Occultation Data in the ECMWF ERA-Interim Re-analysis
SAF/GRAS/METO/REP/GSR/013	ROPP PP validation
SAF/ROM/METO/REP/RSR/014	A review of the geodesy calculations in ROPP
SAF/ROM/METO/REP/RSR/015	Improvements to the ROPP refractivity and bending angle operators
SAF/ROM/METO/REP/RSR/016	Simplifying EGM96 Undulation calculations in ROPP
SAF/ROM/METO/REP/RSR/017	Simulation of L1 and L2 bending angles with a model ionosphere
SAF/ROM/METO/REP/RSR/018	Single Frequency Radio Occultation Retrievals: Impact on Numerical Weather Prediction
SAF/ROM/METO/REP/RSR/019	Implementation of the ROPP two-dimensional bending angle observation operator in an NWP system
SAF/ROM/METO/REP/RSR/020	Interpolation artefact in ECMWF monthly standard deviation plots
SAF/ROM/METO/REP/RSR/021	5th ROM SAF User Workshop on Applications of GPS radio occultation measurements

ROM SAF Reports are accessible via the ROM SAF website: http://www.romsaf.org